

Elasticity measurement of living cells with an atomic force microscope: data acquisition and processing

Philippe Carl · Hermann Schillers

Received: 19 February 2008 / Accepted: 22 April 2008
© Springer-Verlag Berlin Heidelberg 2008

Abstract Elasticity of living cells is a parameter of increasing importance in cellular physiology, and the atomic force microscope is a suitable instrument to quantitatively measure it. The principle of an elasticity measurement is to physically indent a cell with a probe, to measure the applied force, and to process this force-indentation data using an appropriate model. It is crucial to know what extent the geometry of the indenting probe influences the result. Therefore, we indented living Chinese hamster ovary cells at 37°C with sharp tips and colloidal probes (spherical particle tips) of different sizes and materials. We furthermore developed an implementation of the Hertz model, which simplifies the data processing. Our results show (a) that the size of the colloidal probe does not influence the result over a wide range (radii 0.5–26 µm) and (b) indenting cells with sharp tips results in higher Young's moduli (~1,300 Pa) than using colloidal probes (~400 Pa).

Keywords Cystic fibrosis transmembrane conductance regulator · Mechanical properties · Force · Deformability · Membrane strength · Mathematical model

Introduction

Cells are subjected to a complex chemical and mechanical environment. Changes in the physical forces applied to the cells activate cell signaling pathways and induce cytoskeletal rearrangements. Quantifying the mechanical properties of a living cell provides information about the actual condition of the cell and allows a functional characterization of the

cytoskeleton [11, 15, 42, 63]. Many cells such as muscle cells, red blood cells, endothelial cells, and most epithelial cells are continuously squeezed and stretched. These cells need a certain compliance to survive this mechanical stress. In addition, the process of converting physical forces into biochemical signals (mechanotransduction) depends on the elasticity of the cell. A change in cell elasticity to non-physiological values disturbs these mechanisms and may result in a pathophysiological state, i.e., a disease. An increase of cell elasticity was shown for endothelial cells under high sodium conditions [48] and hyperaldosteronism [24, 45], for chondrocytes in arthritis [62], for airway smooth muscle cells in bronchial asthma [2], for erythrocytes in malaria [59], for cardiac muscle in ischemia [19], and several other conditions [34]. A decrease of cell elasticity was shown for cancer cells, e.g., in bladder cancer [35] and breast cancer [21]. In addition, during tissue remodeling and cancer cell migration, the biophysical properties of the extracellular microenvironment are altered [39]. Furthermore, alterations in the stiffness of lipid bilayers are likely to serve as a general mechanism for the modulation of plasma membrane protein function [40]. Among others, G-protein-coupled receptors (GPCRs) play an important role in cellular biomechanics, e.g., sensing mechanical forces like shear stress [7] and modulating the actin cytoskeleton [6]. GPCRs are a 'hot topic' in pharmaceutical research because they are the major target of today's prescription drugs. Elasticity measurements can disclose the specific effects of pharmaceuticals [1, 54, 58] and hormones [24, 25, 46, 47].

In the literature, the biophysical property of a cell is reported as elasticity (elastic modulus), viscoelasticity, and stiffness. Although all of these parameters provide information about the resistance of a material to deformation (the amount of deformation is called the strain), they describe distinctly different properties. (1) A material is said to be elastic if it

P. Carl · H. Schillers (✉)
Institute of Physiology II, University of Münster,
Robert-Koch-Str. 27b, 48149 Münster, Germany
e-mail: schille@uni-muenster.de

deforms under stress (e.g., external forces) and returns to its original shape when the stress is removed. The relationship between stress and strain (force–deformation) is linear, and the deformation energy is returned completely. Elasticity is often referred to as the Young's modulus (E). (2) Viscoelasticity is the property of materials that exhibit both viscous and elastic characteristics when undergoing deformation. Viscosity is a measure of the resistance of a fluid to being deformed by either shear stress or extensional stress. It is the result of the diffusion and interaction of molecules inside of an amorphous material. The reciprocal of viscosity is fluidity. The relationship between stress and strain is non-linear for viscoelastic material, and the deformation energy is not returned completely. The amount of this lost energy is represented by the hysteresis of a loading and unloading cycle (hysteresis in the force–deformation curve). (3) Stiffness is the resistance of a solid *body* to deformation by an applied force.

In general, elastic modulus is not the same as stiffness. Elastic modulus is a property of the constituent material; stiffness is a property of a solid body. The elastic modulus is an intensive property (it does not depend on the size, shape, amount of material, and boundary conditions) of the material; stiffness, on the other hand, is an extensive property (depends on the size, shape, amount of material, and boundary conditions) of the solid body. For example, a solid block and a soft flat spring made from the same material (e.g., steel) have the same elastic modulus but a different stiffness.

The principle of an elasticity measurement is to indent a cell with a probe and measure the applied force. Fitting the force–indentation curve with an appropriate model allows the calculation of the Young's modulus. The Hertz model, developed by Heinrich Hertz in 1882, is widely used. This theory allows a calculation of the components of stress and deformation and gives a relation for elasticity, loading force, indentation, and Young's modulus. This model describes the case of a rigid probe indenting a semi-infinite, isotropic, homogeneous elastic surface. Although the cell is finite, viscoelastic, and anisotropic, these assumptions can be approximately met if the cell is indented slowly enough. Under this condition, viscous contributions are small, and force measurements are dominated by the elastic behavior [38, 43]. It was shown for skeletal muscle cells [10] and airway smooth muscle cells [18] that the normalized viscous dissipation at a probe velocity of 1 $\mu\text{m/s}$ was consistently around 15% of the total energy added. In these studies, condition of low probe velocity minimized viscous losses so that the apparent elastic modulus could be accurately determined.

The Young's modulus describes the tendency of an object to deform along an axis when opposing forces are applied along that axis; it is defined as the ratio of tensile stress to tensile strain. The unit of the Young's modulus (E) is the pascal (Pa). Given the large values typical of many common materials, E is usually quoted in megapascal or

gigapascal, e.g., very soft silicone rubber has 2 MPa, polystyrene has 3 MPa, bone has 17 GPa, enamel (the hardest substance in human body) has 50–84 GPa, steel has 200 GPa, and diamond has 1,100 GPa.

The atomic force microscope (AFM) enables the detection of very small forces and therefore enables quantification of the interaction between a probe and a sample [14, 27]. An AFM equipped with either a sharp tip or a colloidal probe in which the tip is replaced by a sphere [4, 13, 36] has been widely used to measure the mechanical properties of soft materials. The difference between sharp tips and colloidal probes is that a colloidal probe indents a much larger area of the sample than the sharp tip. However, the elasticity of a cell is not homogeneously distributed, i.e., cellular structures such as the cytoskeleton, the nucleus, and the lamellipodia show differences in elasticity. Therefore, a sharp tip rather resolves the local elasticity, while a colloidal probe measures the mechanical properties of virtually the whole cell. Furthermore, a sharp tip is more likely to damage the sample than a colloidal probe, especially at high loading forces.

In the present work, we measured the mechanical properties of living BQ2 cells, a stably cystic fibrosis transmembrane conductance regulator [20, 56] (CFTR)-overexpressing Chinese hamster ovary (CHO) cell line, as a function of the type and size of the colloidal probe. To analyze the acquired data, we calculated the Young's modulus of the cells by an implementation of the Hertz model. An accurate determination of the contact point is crucial for a reliable calculation. The contact point is defined as the point where cantilever deflection starts to rise. Soft samples exhibit a rather small increase in cantilever deflection at low indentations, and, therefore, a clear determination of the contact point is often impossible. The way we have implemented the Hertz model does not require the determination of the position of the contact point and furthermore makes it possible to determine the portion of the curve to be analyzed.

Here, we discuss the validity of the Hertz model applied to living cells and evaluate which Hertz model (cone or sphere) is most suitable.

Materials and methods

Cell cultures

The stably CFTR-overexpressing CHO cell lines, kindly provided by X.-B. Chang and J. Riordan (Scottsdale, AZ, USA), were cultured as previously described [29]. In brief, cells were cultured on glass cover slips (15-mm diameter) and kept at 5% CO_2 at 37°C. The medium consisted of MEM medium supplemented by 80 g/l fetal calf serum, 10 g/l penicillin/streptomycin, and 100 mg/l methotrexate.

The medium was changed every 3 days. Coverslips with confluent cells were used for AFM measurements.

Preparation of colloidal probes

We prepared colloidal probes cantilevers by gluing glass beads with a nominal diameter of 10–30 μm (07668, Polyscience Inc., Warrington, USA) or 30–50 μm (18901, Polyscience Inc. Warrington, USA) on tipless cantilevers (CSC12, MikroMasch, Talin, Estonia). The bead fixation was performed on an inverted microscope (Zeiss Axiovert 25, Zeiss, Oberkochen, Germany) equipped with a micromanipulator (HS6, Märzhäuser, Wetzlar, Germany) and was performed as follows: After fixing a tipless cantilever at the end of the micromanipulator, a thin stripe of freshly prepared two-component glue (Uhu Plus endfest 300, Uhu, Bühl, Germany) was put on a glass slide next to a small amount of beads. We then carefully dipped the cantilever under optical control ($\times 40$ objective) into the glue. This cantilever was then precisely moved on top of a single glass bead and finally approached to the bead until contact was made. Once the cantilever and the bead come in contact, the cantilever is immediately withdrawn. Then, the cantilever is stored for a few hours to allow the glue to reticulate. The size of the glued spheres was subsequently measured using a calibrated inverted microscope (Axiovert 200 with a $\times 100$ 1.45NA Objective, Zeiss, Oberkochen, Germany) with the help of a custom-written plugin (<http://rsb.info.nih.gov/ij/plugins/radial-profile-ext.html>) developed under ImageJ (U.S. National Institutes of Health, Bethesda, MD, USA, <http://rsb.info.nih.gov/ij/>). Colloidal probes with polystyrene beads were purchased from Novascan (Novascan Technologies, Armes, IA, USA).

Elasticity measurements

Elasticity measurements were performed in HEPES buffer (in mM: 140 NaCl; 5 KCl; 5 Glucose; 1 MgCl_2 ; 1 CaCl_2 ; 10 HEPES (*N*-2-hydroxyethylpiperazine-*N'*-2-ethanesulfonic acid); pH=7.4) using a Nanoscope III Multimode-AFM (Veeco Instruments, Santa Barbara, CA, USA). All measurements were carried out in a fluid cell at 37°C (MMFHTR-2 Air and Fluid Sample Heater, Veeco Instruments, Santa Barbara, CA, USA). The different cantilevers used for this work, MLCT (Veeco Probes, Camarillo, CA, USA), CSC12 (MikroMasch, Talin, Estonia), and PT.PS (Novascan Technologies, Armes, IA, USA), were calibrated with a NanoScope V controller (Veeco Instruments, Santa Barbara, CA, USA) by measuring the thermally induced motion of the unloaded cantilever [5, 9, 30, 55]. Spring constants of the used cantilever are summarized in Table 1. Prior to the measurements, we calibrated the cantilever deflection sensitivity on a bare glass coverslip immersed in

Table 1 Summary of the data and comparison of the probes used in this study

	MLCT	Polystyrene	Polystyrene	Glass	Glass	Glass	Glass	Glass
Radius [μm]	0.003	0.5	6.3	6.4	9.5	21.6	26.1	26.4
k [N/m]	0.013	0.014	0.008	0.024	0.088	0.029	0.055	0.022
PLE (SD)	1.93 (0.578)	1.46 (0.213)	1.57 (0.413)	1.46 (0.249)	1.59 (0.255)	1.66 (0.474)	1.71 (0.289)	1.58 (0.377)
E (SD)	1,325 (910.8)	550 (148.9)	242 (49.1)	319 (66.8)	553 (120.5)	400 (159.3)	435 (126.5)	260 (132.1)
n	199	217	154	135	95	99	102	182

k Spring constant, PLE power law exponent, E Young's modulus, n number of indented BQ2 cells

buffer solution. The sensitivity calibration corresponds to the position of the laser on the cantilever and allows calculating the force derived from cantilever deflection using the following equation:

$$\begin{aligned} \text{Force [N]} &= \text{Spring Constant [N/m]} \\ &\times \text{Cantilever Sensitivity [m/V]} \\ &\times \text{Deflection [V]}. \end{aligned} \quad (1)$$

Once the sensitivity calibration had been performed, we withdrew the AFM head and prepared the samples in the following way: Glass cover slips with cells were removed from the culture medium and washed two times with HEPES buffer. The coverslip was glued on metal discs with double adhesive tape and mounted on the AFM. All elasticity measurements were carried out in HEPES buffer at 37°C.

Probes were placed under optical control (OMV-PAL, Veeco Instruments, Santa Barbara, CA, USA) over the center of the cells, and force–distance curves were obtained with a constant approach velocity of 1 $\mu\text{m/s}$. The approach and retraction velocity of the probe is an important parameter for data acquisition since cells appear stiffer at higher velocities [22]. At speeds greater than 10 $\mu\text{m/s}$, the speed-dependent hydrodynamic force acting on the cantilever increases the apparent forces considerably [31]. Furthermore, cells behave in a viscoelastic manner, which means that energy is dissipated into the cell when they are indented by the AFM tip (hysteresis in the force–deformation curve). This hysteresis is minimized at probe velocities at 1 $\mu\text{m/s}$ [37, 43].

Data processing and analysis

All force–deformation data were analyzed with PUNIAS (Protein Unfolding and Nano-Indentation Analysis Software; <http://site.voila.fr/punias>), a custom-built semi-automatic processing and analysis software.

The cantilever deflection resulting from the approach/retraction cycle was monitored as a function of the piezo movement. We then transformed the curves as force versus deformation (δ), the deformation being calculated as follows:

$$\begin{aligned} \text{Deformation [m]} &= \text{Piezo Displacement [m]} \\ &- \text{Cantilever Sensitivity [m/V]} \\ &\times \text{Deflection [V]}. \end{aligned} \quad (2)$$

Data processing and calculation of the Young's modulus are described in detail in the “Results and discussion” section.

Statistics

We used eight different probes in this study, and each probe was used to indent between 95 and 217 cells on two different cell preparations. Mean values \pm SD are reported here. Paired and unpaired *t* tests were performed to test for statistical significance. A *P* value of <0.05 was accepted to indicate significant differences.

Results and discussion

One way to analyze force–deformation data is to calculate the cell's stiffness, namely the slope of the force–deformation curve, which is a parameter reflecting the force, which is needed to indent the sample for a certain depth. The advantage of such an analysis is that it does not require the hypothesis of any model. The drawback of this method is that the geometry or the surface of the indenting probe is not taken into consideration. This means that it is difficult to compare data obtained with different probes. In addition, the fact that a force–deformation curve is not linear over the whole range makes it difficult to set the range where the respective curve should be analyzed.

Hertz model

Another way of analyzing the data is to implement a model such as the widely used Hertz model. It predicts the shape of the contact area for the contact of two bodies, how it grows in size with increasing load, and the magnitude and distribution of surface tractions across the interface. This theory allows a calculation of the components of stress and deformation and gives a relation for elasticity, loading force, indentation, and Young's modulus. The Hertz theory requires some assumptions, e.g., that surfaces are continuous and frictionless and the deformations are small. Although, in the case of cells, these assumptions do not correspond completely to reality, the Hertz model is still useful for achieving information about cell elasticity.

To calculate Young's modulus (*E*) from the force curves, we employed Sneddon's modification of the Hertz model for the elastic indentation of a flat, soft sample by a stiff cone or a stiff sphere [23, 60].

The model relates the applied loading force *f* to the indentation depth or deformation δ .

For a sphere:

$$f_{\text{sphere}} = \frac{4}{3} \frac{E}{1 - \nu^2} \sqrt{R} \delta^{3/2}. \quad (3)$$

For a cone:

$$f_{\text{cone}} = \frac{2}{\pi} \frac{E}{1 - \nu^2} \tan \alpha \delta^2. \quad (4)$$

Here, E is the Young's modulus, ν the Poisson ratio of the sample, R the radius of the sphere, and α the half-opening angle of the sharp tip (35° for MLCT tips). The Poisson's ratio describes the behavior of material upon compression, i.e., the change of transverse strain in relation to the axial strain (in the direction of the applied force). Cells were assumed to be linear elastic, isotropic [64], and incompressible at small strains. Therefore, we used a Poisson ratio of 0.5. For more detailed descriptions, see the reports of Radmacher et al. [12, 53].

Determination of the applicable model

One of the issues in using the Hertz model is to figure out which model (sphere or cone) should be used to analyze the acquired data. This question can be answered by linearization of Eqs. 3 and 4:

$$\log(f_{\text{sphere}}) = \frac{3}{2} \log(\delta) + \log\left(\frac{E}{1-\nu^2} \frac{4}{3} \sqrt{R}\right) \quad (5)$$

$$\log(f_{\text{cone}}) = 2 \log(\delta) + \log\left(\frac{E}{1-\nu^2} \frac{2}{\pi} \tan \alpha\right). \quad (6)$$

These equations are now in the form

$$F = aD + E. \quad (7)$$

In this equation, F is $\log(f_{\text{cone}})$ or $\log(f_{\text{sphere}})$, a is the slope, D is $\log(\delta)$, and E is a function of the Young's modulus. This means that the power law exponent from Eq. 3 or 4 corresponds to the slope of a force–deformation curve plotted in log–log scale. Therefore, a slope of 2 is equivalent to the power law exponent 2 and indicates that the cone model is applicable, while a slope of 1.5 is equivalent to the power law exponent 2 and indicates that the sphere model should be used to calculate the Young's model.

Figure 1 represents the power law exponents obtained using BQ2 cells. It becomes apparent that the power law exponent is close to 1.5 (sphere model) for colloidal probes and close to 2 (cone model) for the sharp tip. There was no significant difference between the polystyrene probe ($6.3 \mu\text{m}$) and the glass probe of comparable size ($6.4 \mu\text{m}$). The standard deviation of the power exponents was in the same range for colloidal probes and the sharp tip. The power law exponents are summarized in Table 1. Proceeding from the results of Fig. 1, we decided to apply the Hertz model with the sphere for the data obtained with colloidal probes and the Hertz model with the cone for the data obtained with sharp tip.

Calculating the Young's modulus

When using the Hertz model for calculating the Young's modulus, there are a certain number of questions to

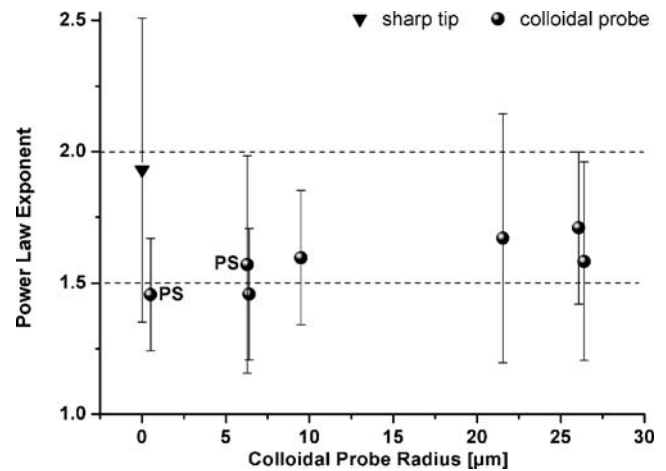


Fig. 1 Measurement of the power law exponent for different sizes of colloidal probes (mean \pm SD, $n=95\text{--}217$) in Chinese hamster ovary cells. The exponent of 1.5 corresponds to the Hertz model using the sphere, while the exponent of 2.0 corresponds to that using the cone (sharp tip). Polystyrene beads are indicated by PS

consider, which may be difficult to answer (besides choosing between the model of 'sphere or cone' to be applied). A major issue is determining the position of the contact point and identifying the portion of the curve, which fits the Hertz model. The Hertz theory requires some assumptions, which do not completely match the reality in the case of cells. Therefore, it is not surprising that a force–deformation curve is only partly in accordance with the Hertz model. To circumvent these difficulties, we implemented a Hertz model in which the determination of the contact point is not necessary and, additionally, the range in which the acquired data fits the Hertz model (allowing the calculation of the Young's modulus) can be found more easily.

We transformed Eqs. 3 and 4 by taking either the power $2/3$ on both sides of the equation in the case of the model with the sphere or the power $1/2$ in the case of the model with the cone so that the dependence of the deformation on the force becomes linear:

$$(f_{\text{sphere}})^{2/3} = \left(\frac{4}{3} \frac{E}{1-\nu^2} \sqrt{R}\right)^{2/3} \delta \quad (8)$$

$$(f_{\text{cone}})^{1/2} = \left(\frac{2}{\pi} \frac{E}{1-\nu^2} \tan \alpha\right)^{1/2} \delta \quad (9)$$

The Young's modulus can be calculated from the slope of the force ^{$2/3$} –deformation curve in the case of the sphere and the force ^{$1/2$} –deformation curve in the case of the cone:

$$\left(\frac{4}{3} \frac{E}{1-\nu^2} \sqrt{R}\right)^{2/3} = \frac{\Delta(f_{\text{sphere}})^{2/3}}{\Delta\delta} = \text{slope} \quad (10)$$

$$\left(\frac{2}{\pi} \frac{E}{1-\nu^2} \tan \alpha\right)^{1/2} = \frac{\Delta(f_{\text{cone}})^{1/2}}{\Delta\delta} = \text{slope} \quad (11)$$

and finally:

$$E = \frac{3}{4} \left(\frac{\Delta(f_{\text{sphere}})^{2/3}}{\Delta\delta}\right)^{3/2} \frac{1-\nu^2}{\sqrt{R}} = \frac{3}{4} \text{slope}^2 \frac{1-\nu^2}{\sqrt{R}} \quad (12)$$

$$E = \frac{\pi}{2} \left(\frac{\Delta(f_{\text{cone}})^{1/2}}{\Delta\delta}\right)^2 \frac{1-\nu^2}{\tan \alpha} = \frac{\pi}{2} \text{slope}^2 \frac{1-\nu^2}{\tan \alpha} \quad (13)$$

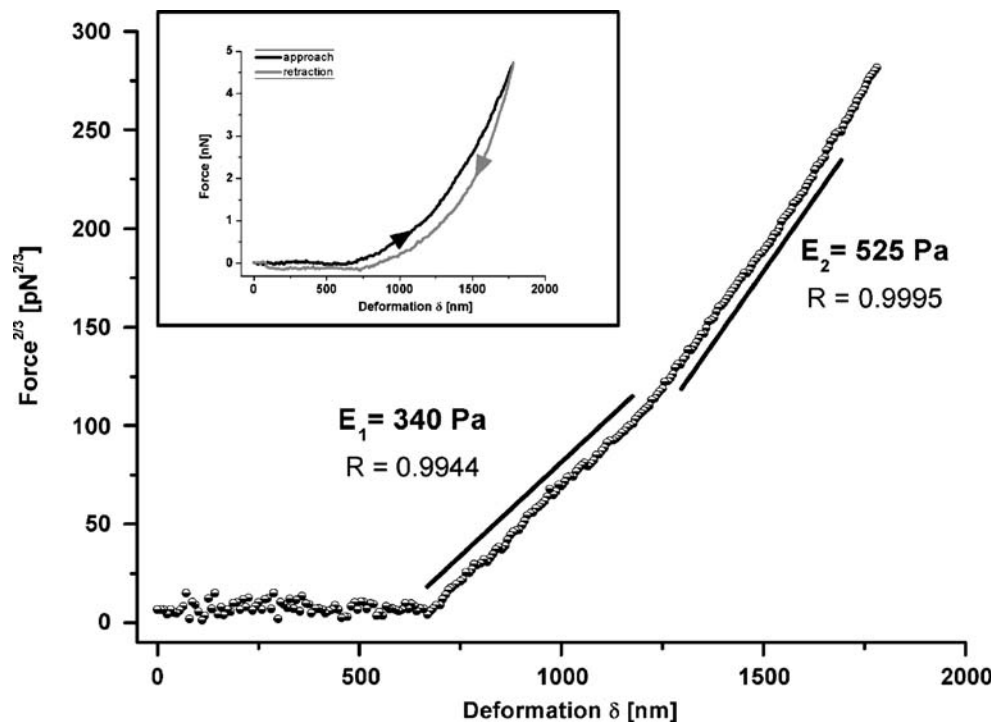
Plotting the indentation data according to the linearized form of the Hertz model (Eq. 8 or 9) should give a straight line provided that the force versus deformation behavior shows a power law dependency in agreement with the given model (bead or cone). This means that the Young’s modulus of the cell is constant over the whole linear range of the curve.

Figure 2 represents the force–deformation curve of a BQ2 cell indented with a colloidal probe ($r=6.4 \mu\text{m}$). Linear regression (least-square fitting) revealed two linear

slopes, i.e., Young’s moduli of the cell, a behavior which is representative for all of our measurements. This means that the Young’s modulus of the cell is not constant over the whole range of indentation. The same observations were made by Kasas et al. and by Sokolov et al. while indenting COS cells [32] and human cervical epithelial cells [61], respectively. These authors considered the cell as a mechanically multilayered structure in which the first layer (the most superficial) represents the actin cytoskeleton [32] or molecular brushes (microvilli, microridges, glycocalyx) [61], and the second layer represents the intermediate filament and microtubule network or “bulky cytosol”. It is likely that in our experiments also that the ‘membrane zone’ (membrane ruffles, cortical actin cytoskeleton, lipid bilayer, membrane proteins) accounts for the first linear slope (E_1) and that the second slope (E_2) is caused by the elasticity of the bulky cytosol (microtubule network, intermediate filament network, cell organelles). We decided to evaluate the first slope because we assumed that a change in elasticity due to physiological/pathophysiological alterations or cell stimulation is more pronounced in the membrane zone than in the bulky cytosol.

Figure 3 represents the values of the Young’s modulus of BQ2 cells measured with probes of different size and material and calculated as described. Obviously, the Young’s moduli obtained with colloidal probes are similar and show an average value of about 400 Pa. These values are independent of the colloidal probes size and composi-

Fig. 2 Force at the power 2/3 versus deformation relationship of a BQ2 cell indented with a colloidal probe ($r=6.4 \mu\text{m}$). Such representation (Eq. 8) of the data reveals two linear regimes (E_1 and E_2) of the curve. The inset shows the force–deformation curve of the same indentation data



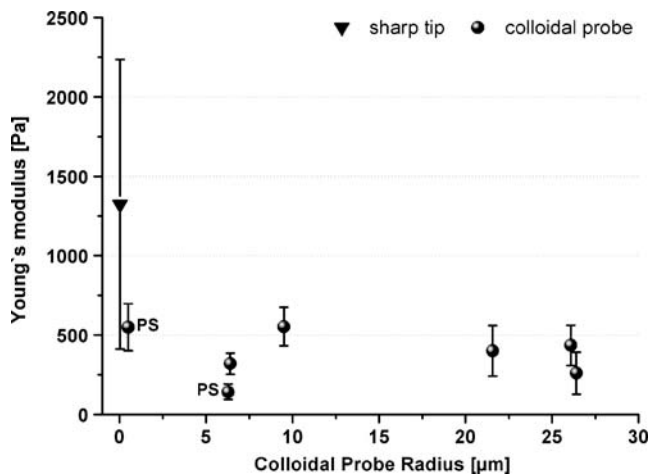


Fig. 3 Measurement of BQ2 Young's modulus for different sizes of colloidal probes calculated with the appropriate Hertz model (mean \pm SD, $n=95$ –217). A colloidal probe size of zero corresponds to the sharp tip, and polystyrene beads are indicated by PS

tion (glass or polystyrene). Our data are in good agreement with the observations of Mahaffy et al. who used polystyrene beads to indent fibroblasts and reported a Young's modulus of 600 Pa for the cell body [41]. Data acquired with a sharp tip result in a Young's modulus, which is about three times higher than the Young's moduli obtained with colloidal probes and, additionally, the standard deviation is remarkably high (Table 1). The latter finding is most likely a result of probing different locations of the cell, e.g., cell nucleus and cell body. For example, in osteoblasts, the cellular elasticity has been shown to vary between 1 kPa in the nuclear area and 100 kPa in the cytoplasmic skirt [8]. Obviously, a sharp tip resolves the local elasticity, a feature which is used in force mapping [44, 49, 53, 57]. A colloidal probe, on the contrary, cannot give a lateral resolution of elasticity but measures the mechanical properties of the whole cell. A dependency of the calculated Young's modulus from this probe type has been described previously. For measurements with sharp tips, Rico et al. found a two times higher Young's modulus for alveolar epithelial cells [50], and Leporatti et al. [36] reported a four times higher Young's modulus for macrophages compared to data obtained with a colloidal probe. In contrast to these results, Engler et al. found no significant differences in the elasticity of medial layers in arterial sections, calculated using data obtained with either sharp tips or colloidal probes [16]. However, our results raise the question whether the Young's moduli obtained with a sharp tip are overestimated or the Young's moduli obtained with a colloidal probe are underestimated. Mechanical properties of cells are determined not only by AFM techniques but also by optical and magnetic tweezers. Optical tweezers use a focused laser beam, and magnetic tweezers use a

magnetic field gradient to provide the attractive or repulsive forces (typically in the order of piconewton) required to hold and move a bead. These techniques can detect lower forces than an AFM cantilever because they have lower spring constants and therefore a higher sensitivity. In magnetic tweezers experiments, a Young's modulus of ~ 400 Pa was reported for human umbilical vein endothelial cells (HUVEC) [17], and ~ 350 Pa was found for macrophages [3]. Optical tweezers studies revealed a Young's modulus of ~ 450 Pa for macrophages [51] and ~ 250 Pa for alveolar epithelial cells [33]. The more common use of sharp tips led to Young's moduli in the range of 1–50 kPa, as shown for platelets [49], HUVEC [25, 26], chicken cardiomyocytes [28], and macrophages [52]. However, significant contributions from the underlying hard substrate are usually expected to occur under the high stresses (>1 kPa) produced by these sharp tips [12]. This would lead to incorrect conclusions concerning the cell elasticities.

From previously published data and our own results (summarized in Table 1), we conclude that colloidal probe indentation, regardless of whether it was performed with AFM or tweezers techniques, produces Young's moduli in the same order of magnitude (<1 kPa), while indentation with sharp tips, probing local mechanical properties of the cell, usually results in higher values. We assume that the results obtained with colloidal probes are closer to the 'true' elasticity because the radius of a sharp tip is smaller by three orders of magnitude compared to a colloidal probe. Therefore, the applied pressure is higher by one order of magnitude in spite of the smaller indentation. Eventually, this leads to locally occurring strain hardening [36]. Additionally, the scatter in the data of Young's moduli is much smaller when using a colloidal probe due to the fact that it does not provide local resolution of elasticity. Another result of our studies is that the size of the colloidal probe in the tested range does not influence the result of elasticity measurements. This adds additional freedom for the researcher to choose the appropriate size of the colloidal probe.

Nevertheless, the biological question should finally determine which type of probe is most applicable. To get local elasticity information (e.g. force mapping), a sharp tip is appropriate, while for the measurement of dynamic changes of whole cell elasticity, a colloidal probe is more suitable.

In summary, the assessment of absolute elasticity values in living cells requires careful selection of the most appropriate type of indentation probe.

Acknowledgments We thank Helga Bertram and Mike Wälte for excellent technical assistance. We thank Hugh de Wardener, St. George's University, London, UK, and Peter Hanley for the critical reading of the manuscript. This work was supported by the Deutsche Forschungsgemeinschaft SFB 629 (A6).

References

- Almqvist N, Bhatia R, Primbs G, Desai N, Banerjee S, Lal R (2004) Elasticity and adhesion force mapping reveals real-time clustering of growth factor receptors and associated changes in local cellular rheological properties. *Biophys J* 86:1753–1762
- An SS, Fabry B, Treppe X, Wang N, Fredberg JJ (2006) Do biophysical properties of the airway smooth muscle in culture predict airway hyperresponsiveness. *Am J Respir Cell Mol Biol* 35:55–64
- Bausch AR, Moller W, Sackmann E (1999) Measurement of local viscoelasticity and forces in living cells by magnetic tweezers. *Biophys J* 76:573–579
- Butt HJ (1991) Measuring electrostatic, van der Waals, and hydration forces in electrolyte solutions with an atomic force microscope. *Biophys J* 60:1438–1444
- Butt H-J, Jaschke M (1995) Calculation of thermal noise in atomic force microscopy. *Nanotechnology* 6:1–7
- Cant SH, Pitcher JA (2005) G protein-coupled receptor kinase 2-mediated phosphorylation of ezrin is required for G protein-coupled receptor-dependent reorganization of the actin cytoskeleton. *Mol Biol Cell* 16:3088–3099
- Chachisvilis M, Zhang YL, Frangos JA (2006) G protein-coupled receptors sense fluid shear stress in endothelial cells. *Proc Natl Acad Sci U S A* 103:15463–15468
- Charras GT, Horton MA (2002) Determination of cellular strains by combined atomic force microscopy and finite element modeling. *Biophys J* 83:858–879
- Cleveland JP, Manne S, Bocek D, Hansma PK (1993) A nondestructive method for determining the spring constant of cantilevers for scanning force microscopy. *Rev Sci Instrum (USA)* 64:403–405
- Collinsworth AM, Zhang S, Kraus WE, Truskey GA (2002) Apparent elastic modulus and hysteresis of skeletal muscle cells throughout differentiation. *Am J Physiol Cell Physiol* 283:C1219–C1227
- Cunningham CC, Gorlin JB, Kwiatkowski DJ, Hartwig JH, Janmey PA, Byers HR, Stossel TP (1992) Actin-binding protein requirement for cortical stability and efficient locomotion. *Science* 255:325–327
- Domke J, Radmacher M (1998) Measuring the elastic properties of thin polymer films with the atomic force microscope. *Langmuir* 14:3320–3325
- Ducker WA, Senden TJ, Pashley RM (1991) Direct measurement of colloidal forces using an atomic force microscope. *Nature* 253:239–241
- Dufrene YF, Hinterdorfer P (2008) Recent progress in AFM molecular recognition studies. *Pflugers Arch* 456:237–245
- Elson EL (1988) Cellular mechanics as an indicator of cytoskeletal structure and function. *Annu Rev Biophys Chem* 17:397–430
- Engler AJ, Richert L, Wong JY, Picart C, Discher DE (2004) Surface probe measurements of the elasticity of sectioned tissue, thin gels and polyelectrolyte multilayer films: correlations between substrate stiffness and cell adhesion. *Surface Science* 570:142–154
- Feneberg W, Aepfelbacher M, Sackmann E (2004) Microviscoelasticity of the apical cell surface of human umbilical vein endothelial cells (HUVEC) within confluent monolayers. *Biophys J* 87:1338–1350
- Fredberg JJ, Jones KA, Nathan M, Raboudi S, Prakash YS, Shore SA, Butler JP, Sieck GC (1996) Friction in airway smooth muscle: mechanism, latch, and implications in asthma. *J Appl Physiol* 81:2703–2712
- Golenhofen N, Redel A, Wawrousek EF, Drenckhahn D (2006) Ischemia-induced increase of stiffness of alphaB-crystallin/HSPB2-deficient myocardium. *Pflugers Arch* 451:518–525
- Greger R, Schreiber R, Mall M, Wissner A, Hopf A, Briel M, Bleich M, Warth R, Kunzelmann K (2001) Cystic fibrosis and CFTR. *Pflugers Arch* 443(Suppl 1):S3–S7
- Guck J, Schinkinger S, Lincoln B, Wottawah F, Ebert S, Romeyke M, Lenz D, Erickson HM, Ananthakrishnan R, Mitchell D, Kas J, Ulvick S, Bilby C (2005) Optical deformability as an inherent cell marker for testing malignant transformation and metastatic competence. *Biophys J* 88:3689–3698
- Hassan E, Heinz WF, Antonik MD, D'Costa NP, Nageswaran S, Schoenenberger CA, Hoh JH (1998) Relative microelastic mapping of living cells by atomic force microscopy. *Biophys J* 74:1564–1578
- Hertz H (1882) Ueber die Berührung fester elastischer Körper. *Reine Angew Mathematik* 92:156–171
- Hillebrand U, Hausberg M, Lang D, Stock C, Riethmuller C, Callies C, Bussemaker E (2008) How steroid hormones act on the endothelium—insights by atomic force microscopy. *Pflugers Arch* 456:51–60
- Hillebrand U, Hausberg M, Stock C, Shahin V, Nikova D, Riethmuller C, Kliche K, Ludwig T, Schillers H, Schneider SW, Oberleithner H (2006) 17beta-estradiol increases volume, apical surface and elasticity of human endothelium mediated by Na⁺/H⁺ exchange. *Cardiovasc Res* 69:916–924
- Hillebrand U, Schillers H, Riethmuller C, Stock C, Wilhelmi M, Oberleithner H, Hausberg M (2007) Dose-dependent endothelial cell growth and stiffening by aldosterone: endothelial protection by eplerenone. *J Hypertens* 25:639–647
- Hinterdorfer P, Dufrene YF (2006) Detection and localization of single molecular recognition events using atomic force microscopy. *Nat Methods* 3:347–355
- Hofmann UG, Rotsch C, Parak WJ, Radmacher M (1997) Investigating the cytoskeleton of chicken cardiocytes with the atomic force microscope. *J Struct Biol* 119:84–91
- Hug MJ, Thiele IE, Greger R (1997) The role of exocytosis in the activation of the chloride conductance in Chinese hamster ovary cells (CHO) stably expressing CFTR. *Pflugers Arch* 434:779–784
- Hutter JL, Bechhoefer J (1993) Calibration of atomic-force microscope tips. *Rev Sci Instrum (USA)* 64:1868–1873
- Janovjak H, Struckmeier J, Muller DJ (2005) Hydrodynamic effects in fast AFM single-molecule force measurements. *Eur Biophys J* 34:91–96
- Kasas S, Wang X, Hirling H, Marsault R, Huni B, Yersin A, Regazzi R, Grenningloh G, Riederer B, Forro L, Dietler G, Catsicas S (2005) Superficial and deep changes of cellular mechanical properties following cytoskeleton disassembly. *Cell Motil Cytoskeleton* 62:124–132
- Laurent VM, Henon S, Planus E, Fodil R, Balland M, Isabey D, Gallet F (2002) Assessment of mechanical properties of adherent living cells by bead micromanipulation: comparison of magnetic twisting cytometry vs optical tweezers. *J Biomech Eng* 124:408–421
- Lee GY, Lim CT (2007) Biomechanics approaches to studying human diseases. *Trends Biotechnol* 25:111–118
- Lekka M, Laidler P, Gil D, Lekki J, Stachura Z, Hryniewicz AZ (1999) Elasticity of normal and cancerous human bladder cells studied by scanning force microscopy. *Eur Biophys J* 28:312–316
- Leporatti S, Gerth A, Kohler G, Kohlstrunk B, Hauschildt S, Donath E (2006) Elasticity and adhesion of resting and lipopolysaccharide-stimulated macrophages. *FEBS Lett* 580:450–454
- Lieber SC, Aubry N, Pain J, Diaz G, Kim SJ, Vatner SF (2004) Aging increases stiffness of cardiac myocytes measured by atomic force microscopy nanoindentation. *Am J Physiol Heart Circ Physiol* 287:H645–H651
- Lu YB, Franze K, Seifert G, Steinhauser C, Kirchhoff F, Wolburg H, Guck J, Janmey P, Wei EQ, Kas J, Reichenbach A (2006) Viscoelastic properties of individual glial cells and neurons in the CNS. *Proc Natl Acad Sci U S A* 103:17759–17764

39. Ludwig T, Kirmse R, Poole K, Schwarz US (2008) Probing cellular microenvironments and tissue remodeling by atomic force microscopy. *Pflugers Arch* 456:29–49
40. Lundbaek JA, Birn P, Girshman J, Hansen AJ, Andersen OS (1996) Membrane stiffness and channel function. *Biochemistry* 35:3825–3830
41. Mahaffy RE, Park S, Gerde E, Kas J, Shih CK (2004) Quantitative analysis of the viscoelastic properties of thin regions of fibroblasts using atomic force microscopy. *Biophys J* 86:1777–1793
42. Martens JC, Radmacher M (2008) Softening of the actin cytoskeleton by inhibition of myosin II. *Pflugers Arch* 456:95–100
43. Mathur AB, Collinsworth AM, Reichert WM, Kraus WE, Truskey GA (2001) Endothelial, cardiac muscle and skeletal muscle exhibit different viscous and elastic properties as determined by atomic force microscopy. *J Biomech* 34:1545–1553
44. Matzke R, Jacobson K, Radmacher M (2001) Direct, high-resolution measurement of furrow stiffening during division of adherent cells. *Nat Cell Biol* 3:607–610
45. Oberleithner H (2007) Is the vascular endothelium under the control of aldosterone? Facts and hypothesis. *Pflugers Arch* 454:187–193
46. Oberleithner H, Ludwig T, Riethmuller C, Hillebrand U, Albermann L, Schafer C, Shahin V, Schillers H (2004) Human endothelium: target for aldosterone. *Hypertension* 43:952–956
47. Oberleithner H, Riethmuller C, Ludwig T, Shahin V, Stock C, Schwab A, Hausberg M, Kusche K, Schillers H (2006) Differential action of steroid hormones on human endothelium. *J Cell Sci* 119:1926–1932
48. Oberleithner H, Riethmuller C, Schillers H, MacGregor GA, de Wardener HE, Hausberg M (2007) Plasma sodium stiffens vascular endothelium and reduces nitric oxide release. *Proc Natl Acad Sci U S A* 104:16281–16286
49. Radmacher M, Fritz M, Kacher CM, Cleveland JP, Hansma PK (1996) Measuring the viscoelastic properties of human platelets with the atomic force microscope. *Biophys J* 70:556–567
50. Rico F, Roca-Cusachs P, Gavara N, Farre R, Rotger M, Navajas D (2005) Probing mechanical properties of living cells by atomic force microscopy with blunted pyramidal cantilever tips. *Phys Rev E Stat Nonlin Soft Matter Phys* 72:021914
51. Rocha MS, Mesquita ON (2007) New tools to study biophysical properties of single molecules and single cells. *An Acad Bras Cienc* 79:17–28
52. Rotsch C, Braet F, Wisse E, Radmacher M (1997) AFM imaging and elasticity measurements on living rat liver macrophages. *Cell Biol Int* 21:685–696
53. Rotsch C, Jacobson K, Radmacher M (1999) Dimensional and mechanical dynamics of active and stable edges in motile fibroblasts investigated by using atomic force microscopy. *Proc Natl Acad Sci U S A* 96:921–926
54. Rotsch C, Radmacher M (2000) Drug-induced changes of cytoskeletal structure and mechanics in fibroblasts: an atomic force microscopy study. *Biophys J* 78:520–535
55. Sader JE (2002) Calibration of atomic force microscope cantilevers. In: Hubbard A (ed) *Encyclopedia of surface and colloid science*. Marcel Dekker, New York, pp 846–856
56. Schillers H (2008) Imaging CFTR in its native environment. *Pflugers Arch* 456:163–177
57. Schneider SW, Matzke R, Radmacher M, Oberleithner H (2004) Shape and volume of living aldosterone-sensitive cells imaged with the atomic force microscope. *Methods Mol Biol* 242: 255–279
58. Schrot S, Weidenfeller C, Schaffer TE, Robenek H, Galla HJ (2005) Influence of hydrocortisone on the mechanical properties of the cerebral endothelium in vitro. *Biophys J* 89:3904–3910
59. Shelby JP, White J, Ganesan K, Rathod PK, Chiu DT (2003) A microfluidic model for single-cell capillary obstruction by *Plasmodium falciparum*-infected erythrocytes. *Proc Natl Acad Sci U S A* 100:14618–14622
60. Sneddon IN (1965) The relation between load and penetration in the axisymmetric boussinesq problem for a punch of arbitrary profile. *Int J Eng Sci* 3:47–57
61. Sokolov I, Iyer S, Subba-Rao V, Gaikwad RM, Woodworth CD (2007) Detection of surface brush on biological cells in vitro with atomic force microscopy. *Appl Phys Lett* 91:023902–1–023902-3
62. Trickey WR, Lee GM, Guilak F (2000) Viscoelastic properties of chondrocytes from normal and osteoarthritic human cartilage. *J Orthop Res* 18:891–898
63. Wang N, Stamenovic D (2000) Contribution of intermediate filaments to cell stiffness, stiffening, and growth. *Am J Physiol Cell Physiol* 279:C188–C194
64. Zhu C, Bao G, Wang N (2000) Cell mechanics: mechanical response, cell adhesion, and molecular deformation. *Annu Rev Biomed Eng* 2:189–226